# Power-law fluid flow simulations using a virtual ghost-cell immersed boundary method

**João Rodrigo Andrade, joao.andrade@etudiant.univ-lille1.fr**[1,2]
**Aristeu Silveira Neto, aristeus@mecanica.ufu.br** [1]
**Daniel Dall'Onder dos Santos, dallonder@ufu.br** [1]

[1]Department of Mechanical Engineering, FEMEC, Federal University of Uberlândia, Fluid Mechanic Laboratory, Campus Santa Mônica, Bloc 5P, Uberlândia, Minas Gerais, Brazil
[2] Laboratoire de Mécanique de Lille (LML), CNRS/FRE 3723, Polytech'Lille, Université des Sciences et Technologies de Lille, Cité Scientifique, Villeneuve d'Ascq, 59655, France

***Abstract:*** *This paper presents the extension of a well-established immersed boundary/ghost-cell approach, the virtual ghost cell, applied to simulate non-Newtonian laminar flows through 2D geometries. This immersed boundary method extends the solution smoothly across the boundary in the same direction as the discretization it will be used for. The ghost cell value is determined locally for each irregular grid cell, making it possible to treat both sharp corners and thin plates accurately. One of the distinguished features of the immersed boundary method here presented is to apply the methodology to the fluid viscosity, a scalar property varying in space and time depending on the shear rate. The choice to simulate power-law fluids is based on its great importance on many industrial processes, mainly in the food, cosmetic and oil industries – it is also the first approach to more complex non-Newtonian fluid models. The time stepping is done using a first order Euler method treating the convective term explicitly and an implicit diffusion term which eliminates the viscous stability constraint. The spatial derivatives are approximated by finite difference method on a staggered, Cartesian and stretched grid method. The central differencing scheme is applied to treat all the terms of momentum equation. This methodology is used firstly to simulate the non-Newtonian flow around a circular cylinder and then a flat plate in a suddenly accelerated unsteady flow.*
***Keywords:*** *immersed boundary method, ghost cell method, power-law fluid*

## 1. INTRODUCTION

Numerical simulation of fluid flow has been a major topic of research in engineering in the past few decades. A major difficulty for the numerical simulation is dealing with complex geometries on different situations as, for example, moving bodies or fluid-structure problems. So far, two different approaches to simulating complex fluid flows have been taken: the unstructured grid method and the immersed-boundary method (IBM). In the latter, a body in the flow field is considered as a kind of momentum forcing in the balance for the momentum equations rather than a real body, and therefore flow over a complex geometry can be easily handled with orthogonal (Cartesian or cylindrical) grids which generally do not coincide with the body surface. The main advantages of the immersed-boundary method are memory and CPU savings and easy grid generation compared to the unstructured grid method (Andrade, 2015).

Many researchers have been using the IBM successfully in various applications covering a broad spectrum of fluid dynamics problems from flow through heart devices (Peskin, 1972, 1977), to the interaction of body movement and fluid flow (Mittal and Iaccarino, 2005), modeling anguilliform swimming (Tyson *et al.*, 2008) and 3-D parachute simulation (Kim and Peskin, 2009). Berthelsen and Faltinsen (2008) presented a virtual ghost-cell, refered as local directional ghost cell approach, for incompressible viscous flow problems with irregular boundaries, where the ghost cell value is determined locally for each irregular grid cell, making it possible to treat both sharp corners and thin plates accurately.

According to Ji *et al.* (2012), the correct calculation of the body force, which represents the fluid-solid boundary conditions, is a key issue for all type of imersed boundary (IB) approaches. Mittal and Iaccarino (2005) classified the IBM in diffuses and sharps methods. One disadvantage with the diffuse methods is that the effect of the boundary is distributed over a band of several grid points which smear out discontinuities across the boundary. This smearing has an unfavorable effect on the accuracy of the numerical scheme (Berthelsen and Faltinsen, 2008) and its consequences can be noted when treating flow over sharp geometry bodies like flat plate, thin airfoil or streamlined bodies, this behavior is better illustrated in Fig. 1. The diffuse methods are considered to be somewhat simpler to use than the sharp category. The sharp kind of method, particularly in three dimensions, implementation is a non-trivial task.

In this work, it is presented the extended form of the local ghost cell (Berthelsen and Faltinsen, 2008) applied to non-newtonian fluid with a semi-implicit temporal integration strategy. Preliminary numerical results of a two-dimensional flow past a stationary circular cylinder at Reynolds number $Re$ = 40 for different power law index are simulated and compared to literature results, also an impulsively started flow past a flat plate at $Re$ = 40 is calculated and a comparison between a shear-thinning, a Newtonian and a shear-thickening fluids is performed.

The present method is based on a finite-difference approach on a staggered grid, an semi-implicit scheme is adopted for all cases. The central difference scheme (CDS) is applied to express both the diffusive and advective contributions of the transport equations on a staggered grid. The fractional-steps (Kim and Moin, 1985) algorithm is used for pressure-velocity coupling.

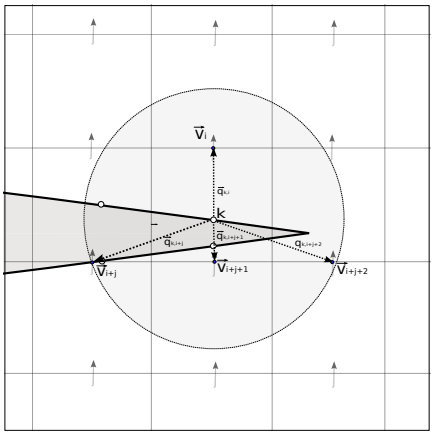


Figure 1: Immersed geometry on a staggered finite volume computational grid showing the illustration of the spreading strategy on the trailing edge of an aerodynamic airfoil. $\vec{q}_{i,j}$ are the vectors from lagragian point to eulerian volumes, $\vec{n}_k$ is the vector normal to the lagrangian surface, $k$ is the lagrangian point and $\vec{v}_i$ are the eulerian velocities.

## 2. MATHEMATICAL AND NUMERICAL MODELING

In this section, the mathematical and numerical procedures chosen to solve the transport equations are described. The laminar two dimensional flow field of incompressible fluid is governed by the momentum balance equations in the inertial frame of reference, in order to solve the flow around an arbitrarily body with complex geometry.

### 2.1 Governing equations for the eulerian domain

A rectangular domain was used for the present simulations and it was discretized with an eulerian grid in a non-uniform cartesian frame. The momentum equations for a viscous incompressible fluid can be written as Eq. 1.

$$\begin{aligned} &\rho\left[\frac{\partial u_i}{\partial t} + \frac{\partial(u_i u_j)}{\partial x_j}\right] = -\frac{\partial p}{\partial x_i} + \frac{\partial}{\partial x_j}\left(\tau_{ij}\right) + f_i. \\ &\frac{\partial u_i}{\partial x_i} = 0, \\ &u_i = u_{i,\Gamma}\ in\ \Omega_\Gamma \end{aligned} \tag{1}$$

where $u_i$ are the components of the velocity vector, $p$ is the kinetic pressure and $\vec{f}_i$ is the eulerian body force. The solid body occupies the domain $\Omega_\Gamma$, with boundary denoted by $\Gamma$ and the surrounding fluid domain denoted by $\Omega_f$. The constitutive equation power-law fluids is given by

$$\tau_{ij} = 2\eta\varepsilon_{ij}, \tag{2}$$

where $\varepsilon_{ij}$ are the strain rate tensor components, related to the velocity field. The viscosity, $\eta$, is given as

$$\eta = m\left(\frac{I_2}{2}\right)^{(n-1)/2} \tag{3}$$

where, $n$ is the power law index, $m$ is the power-law consistency index and $I_2$ is the second invariant of the rate of strain tensor. The Reynolds number in this flow is defined as:

$$Re = \frac{\rho D^n U_0^{2-n}}{m}. \tag{4}$$

### 2.2 Numerical modeling

In this section, the numerical procedures chosen to solve the transport equations are described. The momentum equations are discretized employing the finite-differences method with a staggered arrangement of the velocities and cell-centered arrangement of the pressure variable. The equations are integrated in time using the fractional step method based on the semi-implicit first Euler method, treating the convective term explicitly and an implicitly the diffusion term – which eliminates the viscous stability constraint.

#### 2.2.1 The finite difference method

If the discretization relies on a finite-difference (FD) basis, it is necessary to evaluate vectorial fields coupled to scalar fields, as it is the case when the momentum equations are considered. The issue associated to the positioning of the

primary variables in the computational grid must be carefully accounted. Here, we use a staggered grid, in which the vectorial variables are stored in the grid cell (GC) faces, while the scalars variables are stored in its center. In transient flows the transport equations must be integrated in time as well, which requires the choice of a suitable time marching procedure and brings an important issue associated to the simulation of transient flows: the stability of the numerical scheme.

### 2.2.2 Time-stepping procedure

The equations are integrated in time using the fractional step method (Kim and Moin, 1985; Van-Kan, 1986) which consists three sub-steps. Firstly, a modified momentum equation is solved and an intermediate velocity $u_i^*$ is obtained. A fully implicit scheme is employed for the diffusive terms while the convective terms are discretized using an explicit scheme. In this sub-step, the following modified momentum equation is with an Euler integration scheme:

$$\frac{u_i^* - u_i^n}{\Delta t} = -N\left(u_i^n\right) + L\left(u_i^*\right) + F_i^n \tag{5}$$

where $N\left(u_i^n\right)$ is the convective term and $L\left(u_i^*\right)$ is the diffusive term. For implicit as well as for semi-implicit methods a linear systems of equations needs to be solved for velocity. The second sub-step requires the solution of the pressure correction equation

$$\frac{u_i^{n+1} - u_i^*}{\Delta t} = -\frac{1}{\rho}\frac{\delta p}{\delta x_i} \tag{6}$$

which is solved with the constraint that the final velocity $u_i^{n+1}$ be divergence-free. This gives the following Poisson equation for the pressure correction

$$\frac{\delta}{\delta x_i}\left(\frac{\delta p}{\delta x_i}\right) = \frac{\rho}{\Delta t}\frac{\delta u^*}{\delta x_i} \tag{7}$$

Once the pressure correction is obtained, the velocity is updated as

$$u_i^{n+1} = u_i^* - \frac{\Delta t}{\rho}\frac{\delta p}{\delta x_i} \tag{8}$$

This procedure completes the time step loop. Normally one loop is sufficient to obtain the mass conservation.

### 2.2.3 Spatial discretization of the transport equations

As commented in the introduction of the present section, the central difference scheme (CDS) is applied to express both the diffusive and advective terms of the transport equations. To illustrate the discretization of a derivative using the CDS approach, consider the control cell of lengths $\Delta x_i \times \Delta y_j$, shown in Fig. 2. In such figure, the letters $p_{i,j}$ stand for the center of the cell, whereas the $u_{i,j}$ and $v_{i,j}$ represent the velocities at the faces of the control volume. The

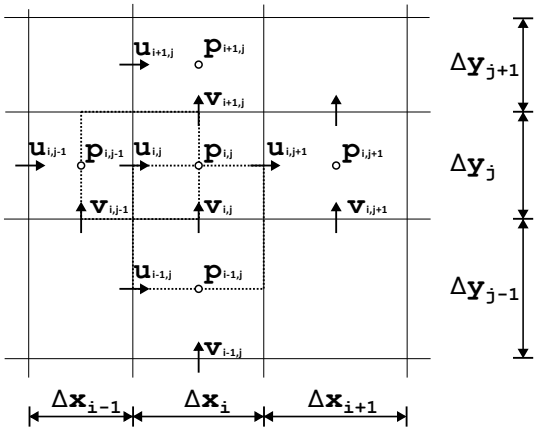


Figure 2: Sketch describing the naming convention and location of velocity components employed in the spatial discretization of the governing equations.

structure adopted for the computational grid can be uniform or non-uniform, so it is necessary to perform interpolations to discretize any spatial derivatives. In the case of non-uniform grids, it is important that such interpolations are obtained using distance-weighted rules (Ferziger and Peric, 1996).

The advective term can be approximated, using the finite-difference method, as:

$$\frac{\partial uu}{\partial x} \approx \frac{u_{i,j+1} + u_{i,j}}{2\left(\Delta x_{i,j} + \Delta x_{i,j-1}\right)}u_{i,j+1} - \frac{u_{i,j-1} + u_{i,j}}{2\left(\Delta x_{i,j} + \Delta x_{i,j-1}\right)}u_{i,j-1} + \frac{u_{i,j+1} - u_{i,j-1}}{2\left(\Delta x_{i,j} + \Delta x_{i,j-1}\right)}u_{i,j} \tag{9}$$

$$\frac{\partial uv}{\partial y} \approx \frac{v_{i+1,j}\Delta x_{i,j-1} + v_{i+1,j-1}\Delta x_{i,j}}{(\Delta x_{i,j} + \Delta x_{i,j-1})(\Delta y_{i,j} + \Delta y_{i+1,j})} u_{i+1,j} - \frac{v_{i,j}\Delta x_{i,j-1} + v_{i,j-1}\Delta x_{i,j}}{(\Delta x_{i,j} + \Delta x_{i,j-1})(\Delta y_{i,j} + \Delta y_{i-1,j})} u_{i-1,j}$$
$$\left[ \frac{(v_{i+1,j}\Delta x_{i,j-1} + v_{i+1,j-1}\Delta x_{i,j})\Delta y_{i+1,j}}{(\Delta x_{i,j} + \Delta x_{i,j-1})(\Delta y_{i,j} + \Delta y_{i+1,j})\Delta y_{i,j}} - \frac{(v_{i,j}\Delta x_{i,j-1} + v_{i,j-1}\Delta x_{i,j})\Delta y_{i-1,j}}{(\Delta x_{i,j} + \Delta x_{i,j-1})(\Delta y_{i,j} + \Delta y_{i-1,j})\Delta y_{i,j}} \right] u_{i,j} \tag{10}$$

The diffusive term can be approximated as:

$$\frac{\partial}{\partial x}\left(\mu \frac{\partial u}{\partial x}\right) \approx \frac{2\mu_{i,j+1}}{\Delta x_{i,j}(\Delta x_{i,j} + \Delta x_{i,j-1})} u_{i,j+1} + \frac{2\mu_{i,j-1}}{\Delta x_{i,j-1}(\Delta x_{i,j} + \Delta x_{i,j-1})} u_{i,j-1}$$
$$- \left[ \frac{2\mu_{i,j-1}}{\Delta x_{i,j}(\Delta x_{i,j} + \Delta x_{i,j-1})} + \frac{2\mu_{i,j+1}}{\Delta x_{i,j-1}(\Delta x_{i,j} + \Delta x_{i,j-1})} \right] u_{i,j} \tag{11}$$

$$\frac{\partial}{\partial y}\left(\mu \frac{\partial u}{\partial y}\right) = \frac{2\mu_{i+1,j}}{\Delta y_{i,j}(\Delta y_{i,j} + \Delta y_{i+1,j})} u_{i+1,j} + \frac{2\mu_{i-1,j}}{\Delta y_{i,j}(\Delta y_{i,j} + \Delta y_{i-1,j})} u_{i-1,j}$$
$$- \left[ \frac{2\mu_{i+1,j}}{\Delta y_{i,j}(\Delta y_{i,j} + \Delta y_{i+1,j})} + \frac{2\mu_{i-1,j}}{\Delta y_{i,j}(\Delta y_{i,j} + \Delta y_{i-1,j})} \right] u_{i,j} \tag{12}$$

The approximations for the $y$-momentum equation is formed in a similar manner.

Finally, boundary conditions must be given in order to solve the set of transport equations. In the developed numerical code of the present work, it is possible to choose between periodicity, Dirichlet, Neumann, or advective boundary conditions (Orlanski, 1976) for each boundary of the computational domain.

Considering the temporal integration method described above and discretization strategy chosen, the result of the numerical form of Eq. 5 is a system of linear algebraic equations of the form

$$A_{i,j}u^*_{i,j} + A_{i+1,j}u^*_{i+1,j} + A_{i-1,j}u^*_{i-1,j} + A_{i,j+1}u^*_{i,j+1} + A_{i,j-1}u^*_{i,j-1} = Q_{i,j}, \tag{13}$$

where $(i, j)$ denotes the node at which the partial differential equation is approximated, the other indexes run over the neighbor nodes involved in finite-difference approximations and $Q_{i,j}$ is the source term depending on the velocity at preceding time step. The source term is composed by both advection and pressure terms.

## 3. IMMERSED BOUNDARY METHOD

The way the boundary conditions are imposed on the immersed boundary determines how an immersed boundary algorithm will look like and it is also what distinguishes one IB method from another. In the present work, Eq. 1(a) will be discretized on a non-boundary conforming cartesian grid and the boundary condition will be imposed directly through modifications of Eq. 13. In general, the modification takes the form of a forcing function in the governing equations that reproduces the effect of the boundary. According to Mittal and Iaccarino (2005), introducing a forcing function leads to a division of IB methods into two groups, namely direct and indirect boundary condition imposition. Another common classification are the continuous and discrete forcing. Herein we use a direct boundary imposition approach.

### 3.1 The virtual ghost cell approach

The present method intends to show a immersed boundary method to solve flows around thin and blunt bodies. The basic idea in this method is to calculate the flow variables adjacent to the immersed boundary with no dependence upon the cells inside the body, such that the boundary conditions in the vicinity of the immersed boundary are satisfied. To apply IBM body forces on thin profile object, a special method is developed to identify surrounding fluid cells nearest to Lagrangian point on the object's surface. The eulerian cells nearing the external surface of the body, need to be identified and its computational stencil must be modified seeking the imposition of the boundary condition.

To identify the immersed boundary influence it is provided three kinds of grid cells which gives rise to boundaries immersed inside the computational domain. The first step of the method is to establish the grid-interface relation with a given immersed boundary description, such as parametrized curve/surface or triangulation. In this step, based on Berthelsen and Faltinsen (2008), all Cartesian grid center nodes are split into the following categories:

1. solid-cells – as the name suggests, are cells whose nodes lie inside the solid body in solid phase;
2. neighboring-cells – grid points in the fluid phase with one or more, depending on discretization order method, neighboring points in the solid phase;
3. fluid-cells – cells whose nodes lie outside the body, in the fluid phase and far from the immersed boundary;
4. forcing-cells (for velocity points) – grid velocity points in the fluid phase with one solid-cell pressure point as neighbor such that the pressure equation can not be applied. This points have its velocities values imposes by interpolation strategy and are not included on the velocity matrix system given by Eq. 13.

According to Linnick and Fasel (2005) and Berthelsen and Faltinsen (2008), Taylor expansions are only valid when applied to continuous and smooth functions. In this sense, methods like finite differences do not presente this characteristics. However, if the function to be considered is piecewise smooth and it is possible to devise a technique that conforms to any jump in the function and its higher derivatives. For simplicity, consider the example given by Berthelsen and Faltinsen (2008): a generic, one-dimensional function $f(x)$ with $x \in [x_{min}, x_{max}]$, which is analytic everywhere except at the interior point $x = x_\alpha$ ( $x_{min} < x_\alpha < x_{max}$),

$$f(x) = \begin{cases} f^-(x) & if\ x_{min} \le x \le x_\alpha \\ f^+(x) & if\ x_\alpha < x \le x_{max}. \end{cases} \tag{14}$$

The grid considered is discretized with uniform grid spacing $\Delta x = (x_{max} - x_{min})/N$, where $[x_{min}, x_{min}]$ are the limits of the computational domain which is discretized into $N + 1$ grid points with uniform grid spacing. For any continuous and smooth region, the numerical approximation to the $n$th-derivative of $f(x_i)$ can be written as

$$f_i^{(n)} = \mathcal{L}^{(n)}(f_l, f_{l+1}, ..., f_i, ..., f_{r-1}, f_r) + \mathcal{O}(\Delta x^p), \tag{15}$$

where $\mathcal{L}$ denotes the discrete finite difference operator and $p$ is the order of accuracy of the numerical approximation.

If there is a discontinuity located at $x_\alpha$, the finite difference must be modified, because it involves grid cells on both sides of the discontinuity point. A remedy to deal with this problems is that, since $f(x)$ is piecewise analytic, the derivative operator can be applied considering only the cells values at one side of the discontinuity by considering a smoothly extension beyond the interface by means of a fictitious domain. So, the standard finite difference operator $\mathcal{L}^{(n)}$ can be can be applied to approximate the $n$th-derivative of $f(x_i)$:

$$f_i^{(n)} = \mathcal{L}^{(n)}(f_l, f_{l+1}, ..., f_i, ..., f_j, f_{j+1}^g, ..., f_{r-1}^g, f_r^g) + \mathcal{O}(\Delta x^p), \tag{16}$$

where the function values $f_{j+1}, ..., f_r$ are replaced by fictitious ghost cell values $f_{j+1}^g, ..., f_r^g$. The ghost cell values can be determined by, for instance, fitting a $q$th order Lagrange polynomial.

Based on the above equations, a relationship between the grid and the immersed boundary needs to be established for the momentum equation. Based on the equating introduced by Berthelsen and Faltinsen (2008), the cells located close to an immersed boundary, Eqs. 13 and 15, are no long valid and may be modified by replacing any point separated by an immersed boundary by a temporary fictitious value. This smoothly extends the solution across the boundary and the effect of the body inside the flow can be well represented. For instance, if on the stencil of a cell velocity point $u_{i,j}$, the velocities points $(i, j+1/2)$ and $(i+1/2, j)$ lying inside the immersed boundary can not be used to evaluate the cell $(i, j)$. Using the strategy depicted above, this solid-cells velocities points will be replaced by values obtained by extrapolating the solution along the $x$ and/or $y$-direction:

$$u_{i+1,j}^g = \alpha_0 + \alpha_1 u_{i,j} + \alpha_2 u_{i-1,j} + \alpha_3 u_\Gamma \tag{17}$$

and

$$u_{i,j+1}^g = \beta_0 + \beta_1 u_{i,j} + \beta_2 u_{i,j-1} + \beta_3 u_{i-1,j+1} + \beta_4 u_{i-2,j+1} + \beta_5 u_\Gamma \tag{18}$$

where $u_\Gamma$ is the velocity at the boundary. For this case, the coefficients from Eq. 13 are replaced by

$$A_{i,j}^g u_{i,j}^* + A_{i-1,j}^g u_{i-1,j}^* + A_{i,j-1}^g u_{i,j-1}^* + A_{i-1,j+1}^g u_{i-1,j+1}^* + A_{i-2,j+1}^g u_{i-2,j+1}^* = Q_{i,j}^g, \tag{19}$$

where

$$\begin{aligned} A_{i,j}^g &= A_{i,j} + A_{i+1,j}\alpha_1 + A_{i,j+1}\beta_1, \\ A_{i,j-1}^g &= A_{i,j-1} + A_{i,j+1}\beta_2, \\ A_{i-1,j} &= A_{i-1,j} + A_{i+1,j}\alpha_2, \\ A_{i-1,j+1} &= A_{i,j+1}\beta_3, \\ A_{i-2,j+1} &= A_{i,j+1}\beta_4, \end{aligned} \tag{20}$$

To obtain the ghost cell values, a third order Lagrange cubic extrapolation polynomial scheme is used. For Poisson equation for pressure, the same procedure is made: internal cells are replaced by ghost values depending on fluids cells. More details about velocity and pressure equations can be found in Berthelsen and Faltinsen (2008).

With regard to the non-newtonian fluid viscosity, the strain rate tensor components need to be calculated in the whole domain. For the calculation cells close to the immersed boundary, a procedure similar to velocity and pressure points was used, however a first order polynomial scheme is considered. For instance, if on the calculation of the velocity gradient $(\partial u/\partial x)_{i,j}$ in cell $i, j$, the velocity value at point $(i, j + 1)$ lies inside the solid phase, a ghost value may be used since this point is not in the fluid domain, such that:

$$u_{i,j+1}^g = \alpha_0 + \alpha_1 u_{i,j} + \alpha_\Gamma u_\Gamma \tag{21}$$

and the velocity partial derivative $(\partial u/\partial x)_{i,j}$ is computed as

$$\frac{u_{i,j+1/2}^g - u_{i,j-1/2}}{\Delta x_{i,j}} = \frac{(\alpha_0 + \alpha_1 u_{i,j} + \alpha_\Gamma u_\Gamma) - u_{i,j-1/2}}{\Delta x_{i,j}} \tag{22}$$

## 4. Results

Two different geometries are investigated and both are calculated at $Re = 40$ for different power law indexes. The circular cylinder results are compared to the literature (Soares *et al.*, 2005; Bharti *et al.*, 2008; Patnana *et al.*, 2009) in order to validate the method. Drag and pressure coefficients were calculated and are defined as $C_D = 2F_D/(\rho U_0^2 d)$ and $C_P = 2(P - P_0)/\rho U_0^2$, respectively, where $F_D$ is the drag force. In all simulated cases, a domain with $W/D = 60$, $L/D = 120$ is adopted, where $L$ is the domain horizontal length, $W$ is the vertical length and $D$ is the characteristic length. Dirichlet boundary conditions are used at the inflow $(u/u_\infty = 1; v = 0)$ and at the cylinder surface $(u = 0, v = 0)$; a Neumann-type boundary condition is adopted at the outflow and farfield boundaries.

### 4.1 Laminar flow past a 2D stationary circular cylinder

Laminar flows past a two-dimensional stationary circular cylinder, a classic benchmark problem, are simulated to verify the method presented in this work. For the simulations at $Re = 40$, the power law index $(n)$ is varyed from $0.4$ to $1.4$ and a computational mesh of $100,000$ volumes is used. Figure 3 shows the sketch of the computational domain.

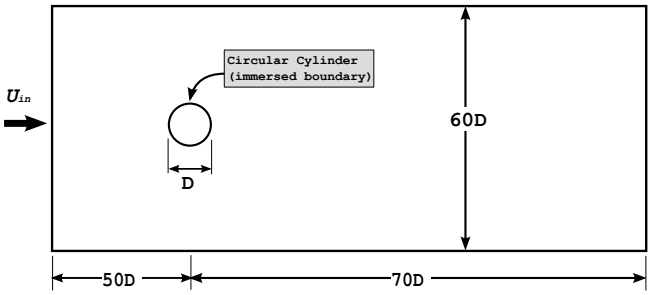


Figure 3: Schematics of the unconfined flow around a circular cylinder.

The comparison of the drag coefficient obtained in the present work with other numerical and experimental results is presented in Tab. 1. It can be observed that good agreement was obtained.

Table 1: Drag coefficient $(C_D)$ for steady uniform flow past a circular cylinder for $Re = 40$.

| | $n = 0.4$ | $n = 0.8$ | $n = 1.4$ |
|---|---|---|---|
| Present Study | 1.2521 | 1.4832 | 1.6413 |
| Soares *et al.* (2005) | – | 1.4900 | 1.6200 |
| Bharti *et al.* (2008) | – | 1.4173 | 1.5438 |
| Patnana *et al.* (2009) | 1.2459 | – | 1.6541 |

Figure 4 shows the influence of the power law index over the pressure coefficient, vorticity and drag coefficient. The results are in accordance with the related non-Newtonian fluids literature, where the pressure and drag coefficients, respectively depicted in Figs. 4a and 4b for different cyilinder surface positions, are increased due to the rise in the fluid viscosity when the $n$ index is varyed from $0.4$ to $1.0$. For the same reason, the vorticity (Fig. 4b) decreases when the fluid becomes less pseudoplastic.

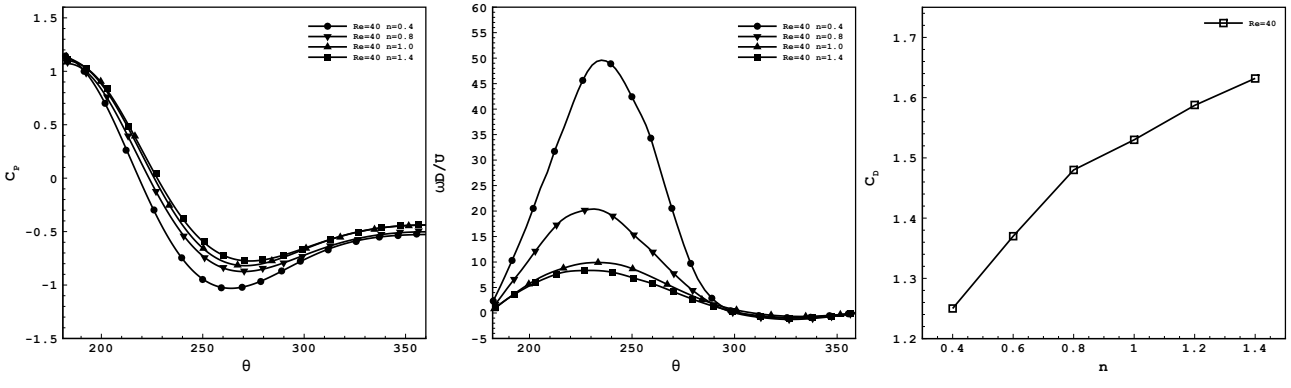


(a) (b) (c)

Figure 4: Effect of $n$ on the variation of the (a) pressure coefficient $C_p$ and (b) vorticity $(\omega D/U)$ on the surface of the cylinder and (c) on total drag coefficient $(C_D)$.

Figures 5 and 6 show, for $n = 0.4$ and $n = 1.2$ respectively, the streamlines, iso-vorticity contours and iso-viscosity fields. The wake formed behind the cylinder attains a steady symmetric state for these cases, which is in agreement with

the well-established result by the linear stability theory. The vortices behind the cylinder increases with the power law index once the same boundary conditions are prescribed for both simulations. The increase in the viscosity leads to a an increase of the diffusive effect – the presence of the cylinder is conveyed downstream through the flow.

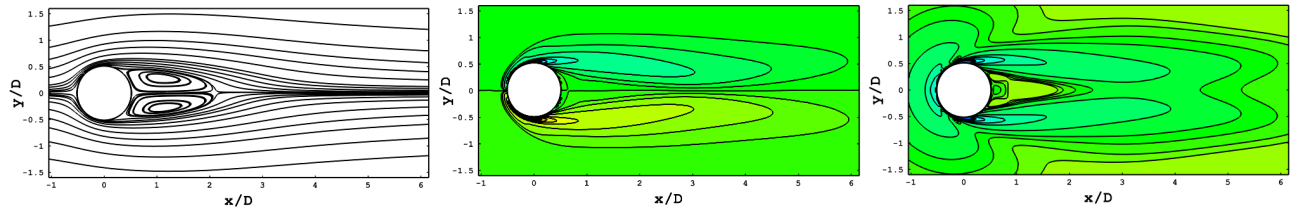


(a) (b) (c)

Figure 5: Near wake structure of (a) streamlines, (b) iso-vorticity contours and (c) iso-viscosity contours for $Re$ = 40 and $n$ = 0.4.

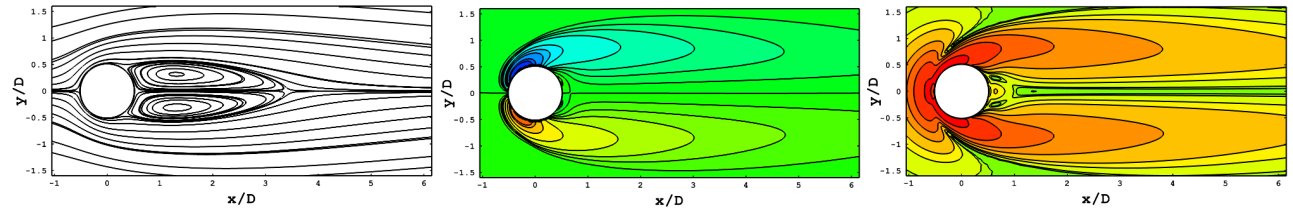


(a) (b) (c)

Figure 6: Near wake structure of (a) streamlines, (b) iso-vorticity contours and (c) iso-viscosity contours for $Re$ = 40 and $n$ = 1.4.

### 4.2 Suddenly accelerated normal flat plate

In this section, the results for the flow past a suddenly accelerated vertical flat plate are presented for $Re$ = 40 and power-law index equal to 0.8, 1.0 and 1.2. Differently from the cylinder, this geometry is subjected to an unsteady flow – the results shown here are obtained for $tU/D$ = 1. However, the computational setup is identical to the previous example, where the circular cylinder is replaced by an infinite thin plate oriented normal to the flow (Fig. 7). To discretize the geometry, a computational mesh of 150, 000 volumes is used.

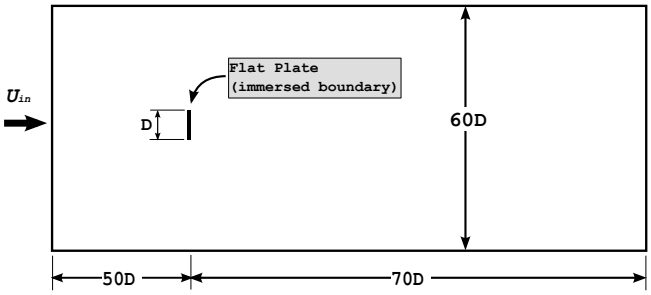


Figure 7: Schematics of the unconfined flow around a flat plate.

Figures 8, 9 and 10 present the streamlines, iso-vorticity and iso-viscosity contours for the three simulated flows. It can be noticed that for the rheological parameters employed, there is almost no noticeable difference between the vortices downstream the cylinder. This is also observed when the iso-vorticity figures are taken into account. The viscosity fields are more sensitive to the effects of the power-law index variation. For the smaller $n$, a smooth variation of the viscosity values is observed, while for $n$ = 1.2 there are strong viscosity gradients. It is important to mention that the Newtonian model is recovered when $n$ = 1.0. Regarding on the drag coefficient, for both $n$ = 0.8 and $n$ = 1.0, the estimated values are the same $C_D$ = 2.92; for $n$ = 1.2, the value is 2.94.

## 5. FINAL REMARKS

An immersed boundary method for solving the incompressible momentum equation in irregular domains with a power-law fluid has been presented. The solid boundary has been treated by a local one-dimensional ghost cell approach. The local feature of the present method allows for highly irregular boundaries (e.g. sharp corners) to be treated accurately. We have applied the present technique to two test problems involving steady and unsteady flow past stationary objects. This

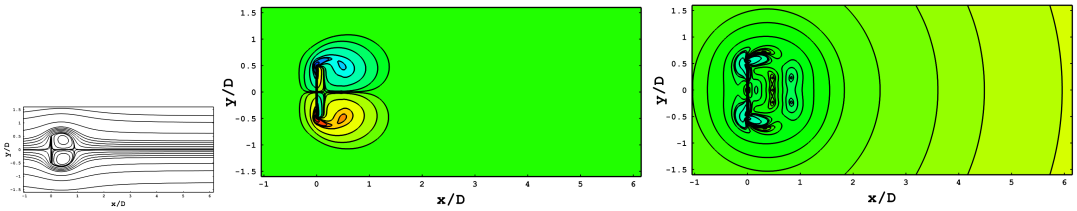


(a) (b) (c)

Figure 8: Near wake structure of (a)-streamline, (b)-iso-vorticity contours and (c)-iso-vorticity contours at $Re$ = 40 and $n$ = 0.8.

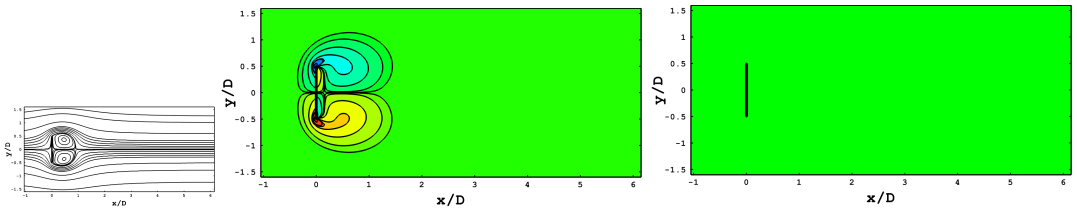


(a) (b) (c)

Figure 9: Near wake structure of (a)-streamline, (b)-iso-vorticity contours and (c)-iso-vorticity contours at $Re$ = 40 and $n$ = 1.0.

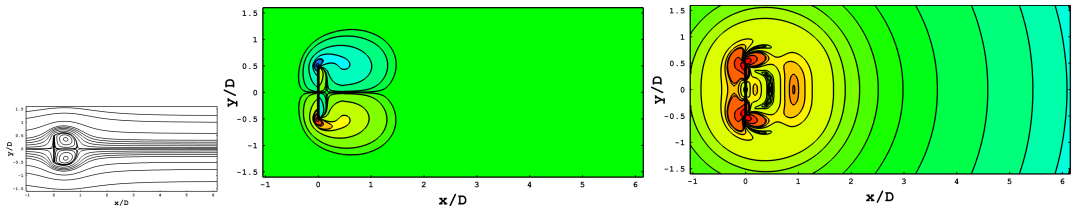


(a) (b) (c)

Figure 10: Near wake structure of (a)-streamline, (b)-iso-vorticity contours and (c)-iso-vorticity contours at $Re$ = 40 and $n$ = 1.2.

includes uniform flow past a circular cylinder and an impulsively started flow past a flat plate. For the uniform flow past a circular cylinder and the impulsively started flow, it is shown that the method is capable of well represent the geometry tested. The calculated force coefficients are found to be well within the range of data reported by other works.

## 6. ACKNOWLEDGEMENTS

The authors acknowledge CNPQ, CAPES, PROEX, PROPP, FAPEMIG and PETROBRAS for the financial support and the School of Mechanical Engineering of the Federal University of Uberlândia for the technical support.

## 7. REFERENCES

Andrade, J.R., 2015. *Immersed Boundary Methods for sharp-shaped geometries: implementation and validation (In Portuguese).* Master's thesis, Programa de Pós Graduação em Engenharia Mecânica da Universidade Federal de Uberlandia.

Berthelsen, P.A. and Faltinsen, O.M., 2008. "A local directional ghost cell approach for incompressible viscous flow problems with irregular boundaries." *Journal of Computational Physics*, Vol. 227, 4354-4397.

Bharti, R.P., Chhabra, R.P. and Eswaran2, V., 2008. "Steady flow of power law fluids across a circular cylinder." *The Canadian Journal of Chemical Engineering*.

Ferziger, J. and Peric, M., 1996. *Computational Methods for Fluid Dynamics*. [S.l.]: Springer.

Ji, C., Munjiza, A. and Williams, J., 2012. "A novel iterative direct-forcing immersed boundary method and its finite volume applications". *Journal of Computational Physics*, Vol. 231:1797-1821.

Kim, J. and Moin, P., 1985. "Application of a fractional step method to incompressible navier-stokes equations." *J. Comp. Physics*, Vol. 59, 308.

Kim, Y. and Peskin, C.S., 2009. "3-d parachute simulation by the immersed boundary method." *Computational Fluids*, Vol. 38:1080-90.

Li, Z., 2003. "An overview of the immersed interface method and its applications." *Taiwanese J. Math.*, Vol. 7, 1–49.

Linnick, M.N. and Fasel, H., 2005. "A high-order immersed interface method for simulating unsteady compressible flows on irregular domains." *J. Comput. Phys.*, Vol. 204:157-192.

Mittal, R. and Iaccarino, G., 2005. "Immersed boundary methods". *Annual Reviews of Fluid Mechanics*, Vol. 37, 239-261.
Patnana, V.K., Bharti, R.P. and Chhabra, R.P., 2009. "Two-dimensional unsteady flow of power-law fluids over a cylinder." *Chemical Engineering Science*, Vol. 64, 2978 - 2999.
Peskin, C., 1972. "Flow patterns around heart valves: A numerical method." *Jounal of Computational Physics*, Vol. 10:252-271.
Peskin, C., 1977. "Numerical analysis of blood flow in the heart." *Jounal of Computational Physics*, Vol. 25:220-52.
Soares, A.A., Ferreira, J.M. and Chhabra, R.P., 2005. "Flow and forced convection heat transfer in cross flow of nonnewtonian fluids over a circular cylinder." *Ind. Eng. Chem. Res.*, Vol. 44, 5815–5827.
Tyson, R., Jordan, C.E. and Hebert, J., 2008. "Modelling anguilliform swimming at intermediate reynolds number: a review and a novel extension of immersed boundary method applications." *Computational Methods for Applied Mechanical Engineering*, Vol. 197:2105-18.
Van-Kan, J., 1986. "A second-order accurate pressure-correction scheme for incompressible viscous flow". *J. Sci. Stat. Comput.*, Vol. 7, pp. 870–891.

## 8. RESPONSIBILITY NOTICE

The authors are the only responsible for the printed material included in this paper.